Composites Part A 125 (2019) 105542

Contents lists available at ScienceDirect

Composites Part A

journal homepage: www.elsevier.com/locate/compositesa

Comprehensive study of effects of filler length on mechanical, electrical, and thermal properties of multi-walled carbon nanotube/polyamide 6 composites

Han Gyeol Jang[a,1], Beomjoo Yang[b,1], Myung-Seob Khil[c], Seong Yun Kim[c,*], Jaewoo Kim[a,*]

[a] Institute of Advanced Composite Materials, Korea Institute of Science and Technology (KIST), 92 Chudong-ro, Bongdong-eup, Wanju-gun, Jeonbuk 55324, Republic of Korea
[b] School of Civil Engineering, Chungbuk National University, 1 Chungdae-ro, Seowon-gu, Cheongju, Chungbuk 28644, Republic of Korea
[c] Department of Organic Materials and Fiber Engineering, Chonbuk National University, 567 Baekje-daero, Deokjin-gu, Jeonbuk 54896, Republic of Korea

ARTICLE INFO

Keywords:
A. Polymer-matrix composites (PMCs)
B. Mechanical properties
B. Thermal properties
B. Electrical property

ABSTRACT

In spite of active studies on multi-walled carbon nanotube (MWCNT)-incorporated polymer, MWCNTs of different thickness and lengths have been employed. Here, the effects of MWCNT morphology, specifically its length, on the mechanical, thermal, and electrical properties of MWCNT/polymer composites were examined in comparison with theoretical modeling. Field-emission scanning electron microscopy and micro-computed tomography observations revealed that short MWCNTs were dispersed more uniformly than long MWCNTs in a polyamide 6 (PA6) polymer. Correlation of this result with the tensile performance revealed that at low MWCNT concentrations the long-MWCNT/PA6 composite showed superior tensile properties since the effect of length was dominant. However, at high MWCNT concentrations, the short-MWCNT/PA6 showed superior tensile properties to the long-MWCNT/PA6 due to the better dispersion of the former. The thermal conductivity gradually improved with increasing MWCNT concentration, showing larger improvement for the long-MWCNT/PA6, while the electrical conductivity reached percolation threshold at 1 wt% for both MWCNTs.

1. Introduction

Multi-walled carbon nanotubes (MWCNTs) have been used as an effective filler in polymer composites on account of their high aspect ratio, low density, excellent mechanical strength, and high thermal and electrical conductivities [1]. Polymer materials have also been widely used owing to their low weight and reasonable cost, but they suffer from drawbacks of inferior mechanical properties and poor thermal and electrical conductivities compared to metals. Therefore, continued efforts have been made over the decades to improve polymer properties through incorporation of MWCNTs [2].

A polymer composite with MWCNTs incorporated as a filler has been extensively studied in various fields, particularly for mechanical, thermal, and electrical applications [3–5]. Since a polymer possesses relatively poor mechanical properties, the incorporation of MWCNTs can greatly enhance the strength and fracture resistance of the polymer [6,7]. A polymer usually has a very short phonon mean free path, and its thermal conductivity is much lower than 1 W/m K [8–10]. Thus, its heat radiation performance can be improved via the creation of a heat conduction path through the incorporation of thermally conductive MWCNTs. In the same manner, an electrical path can be created in a polymer via the incorporation of MWCNTs, which possess high electrical conductivity. When a certain concentration of MWCNTs is uniformly dispersed in a polymer, the percolation threshold is reached since the MWCNTs are close enough for the occurrence of electron flow via the tunneling effect [11].

Extensive research has been conducted on the MWCNT-incorporated polymer composites [12–17], specifically the effects of MWCNT on composite properties. Consequently, the MWCNT/polymer composites have been successfully applied in various fields such as sporting goods, electronic devices, and ESD shields [18]. However, the comprehensive understanding of these composites is still restricted by the differences in MWCNTs used in each research. Furthermore, there is still a lack of research on composite materials with high filler loading. Therefore, it would be beneficial if the dependence of mechanical, electrical, and thermal performance on MWCNT filler is systematically

* Corresponding authors.
E-mail addresses: sykim82@jbnu.ac.kr (S.Y. Kim), jaewoo96@kist.re.kr (J. Kim).
[1] These authors contributed equally to this work.

https://doi.org/10.1016/j.compositesa.2019.105542
Received 5 April 2019; Received in revised form 16 July 2019; Accepted 17 July 2019
Available online 19 July 2019
1359-835X/

examined for a single well characterized system. In combination with experimental observations, theoretical interpretation will also help to gain a deeper understanding of the MWCNT/composite and simultaneously develop its design rule.

In this study, two types of MWCNTs with similar surface chemistry and thickness but with different lengths were incorporated into polyamide 6 (PA6) polymer, and composites were prepared by a melt-compounding method in order to study the effects of morphological changes, specifically alteration of the MWCNT length, on the composite properties. The degree of dispersion of MWCNTs in the composite was measured as a function of the MWCNT length through two-dimensional field-emission scanning electron microscopy (2D FE-SEM) and non-destructive three-dimensional micro-computed tomography (3D micro-CT). Finally, the effects of the length and degree of dispersion of MWCNTs on the composite properties were comprehensively examined by measuring the tensile performance, electrical conductivity, and thermal conductivity. For deeper understanding, theoretical modeling and analysis were carried out and compared with experimental observations.

2. Experimental

2.1. Materials and composite fabrication

Two types of MWCNTs of similar diameters (7–10 nm) but different lengths were used as fillers. Following manufacturer specifications [19], short MWCNTs (Jenotube 9, Jeio Co., Incheon, Korea) and long MWCNTs (Jenotube 8, Jeio Co., Incheon, Korea) had lengths of 10–50 and 100–200 μm, respectively, which corresponds to a 5-fold difference in their average lengths. A PA6 pellet (KN111, Kolon Plastics, Inc., Gwacheon, Korea) was used as a polymer matrix. All reagents were used without further purification.

To minimize the effect of moisture, the MWCNT filler and PA6 matrix were dried in a convection oven at 80 °C for 5 h prior to mixing. Composites were prepared by adding 1, 3, 5, 7, and 10 wt% MWCNTs to the PA6 polymer, and a Haake Rheomix internal mixer (HAAKE™ Rheomix 600R OS Mixer, Thermo Scientific, Inc., GA, USA) was used for melt-compounding at a screw speed of 60 rpm for 30 min. The mixture was molded at 250 °C and 20 MPa for 15 min by the use of a heating press (D3P-30J, Daheung Science, Incheon, Korea), cooled to room temperature using cooling water, and then removed from the press. A flat plate with dimensions of $2 \times 25 \times 25\ mm^3$ was used as the specimen for thermal and electrical conductivity measurements. As a specimen for tensile tests, a flat plate with dimensions of $1 \times 200 \times 200\ mm^3$ was cut into a dog-bone shape using a waterjet (Mach 300, TOPS Co., Gimhae, Korea) according to the ASTM D638 standard (type V). Tensile specimens with 10 wt% MWCNTs could not be manufactured, because they crumbled during molding using the heating press. Fig. S1 shows detailed images and dimensions of the specimens used to measure tensile performance, thermal conductivity, and electrical conductivity.

2.2. Spectroscopic characterization of MWCNTs

The MWCNTs and their dispersion state in the composites were measured using a field-emission scanning electron microscope (Nova NanoSEM 450, FEI Co., OR, USA) operated at 10 kV in a nitrogen atmosphere. MWCNTs were dispersed via ethanol sonication in an ultrasonic bath (JAC-2010P, Kodo Technical Research Co., Ltd., Hwaseong, Korea) for 1 h and then coated on a Si wafer for 30 s at a speed of 3000 rpm by means of a spin coater (Spin-3000D, MIDAS System, Daejeon, Korea). The prepared MWCNT/PA6 composite specimens were fractured into small pieces in liquid nitrogen and then platinum-coated for 120 s under vacuum by means of a sputter coating machine (Ion Sputter E-1030, Hitachi High Technologies, Tokyo, Japan).

The micro-computed tomograph (Skyscan 1172, Bruker Co., MD, USA) was operated under X-ray conditions of 51 kV and 194 mA to measure the 3D dispersion state of the MWCNTs in the composite. The micro-CT specimen had dimensions of $1 \times 2 \times 2\ mm^3$. A series of cross-sectional images were reconstructed in three dimensions using the NRecon program, and the dispersion state of the MWCNTs in the composite was analyzed using the CTVox program.

For analysis of the structural defects and surface chemical properties of the MWCNTs, they were dried overnight in a vacuum oven at 80 °C to minimize the effect of moisture. For analysis of structural defects, dried MWCNTs were attached on a slide glass using a carbon tape and measured using a Raman spectroscope (LabRAM HR 800, Horiba Jobin Yvon, Kyoto, Japan) equipped with a 514 nm Ar-ion laser at room temperature and atmospheric pressure. For analysis of surface chemistry, the MWCNTs were mixed with KBr, pressed into a plate shape, and then characterized by Fourier transform infrared (FT-IR) spectroscopy (Nicolet 6700, Thermo Scientific, Inc., MA, USA) in a frequency range of 4000 to 500 cm^{-1} at a resolution of 1 cm^{-1}.

2.3. Mechanical, thermal, and electrical characterization of composite

The tensile properties of the composite were measured using a universal testing machine (Instron 5567, Instron Corp., MA, USA) equipped with a 3 kN load cell. A pneumatic grip was used to prevent any slippage, and dog-bone-shaped specimens were stretched at a crosshead displacement speed of 5 mm/min at room temperature and atmospheric pressure. The isotropic thermal conductivity of the composite was measured at room temperature and atmospheric pressure according to the ISO 22007-2 standard by use of a conductivity-measuring instrument (TPS 2500 S, Hot Disk AB, Gothenburg, Sweden) with a 7531 sensor made of thin nickel wire. The electrical conductivity of the composite was measured at room temperature by the four-probe method according to ASTM D257 (FPP-RS8, DASOL Eng., Cheongju, Korea). The resistance R was calculated using the output current and voltage drop via the following equation:

$$R = \frac{\Delta V w t}{i L} \tag{1}$$

where ΔV and i denote the voltage drop over a distance of 6 mm and the output current, respectively. w, t, and L denote the width, thickness, and length, respectively, of the specimen. The electrical conductivity was determined as the reciprocal of the calculated resistance value.

2.4. Theoretical modeling and analysis

To deeply examine the present experimental studies, theoretical simulations and analysis were performed on the tensile strength, Young's modulus, thermal conductivity, and electrical conductivity of MWCNT/PA6 composites. The tensile strength and Young's modulus were calculated through the modified Halpin-Tsai, while the thermal and electric conductivities were simulated via micromechanics-based ensemble volume average method and effective medium theory, respectively.

3. Results and discussion

3.1. Long versus short MWCNTs

As shown in the SEM images in Fig. 1(a) and (c), the two types of MWCNTs used in this study were observed as bundles, wherein multiple strands of MWCNTs were longitudinally entangled. Their bundle lengths were 180 and 10 μm, differed by a factor of 18. Considering the manufacturer's specifications of a 5-fold difference in their average lengths, this might indicate more entanglement for long MWCNTs. The diameter of the MWCNT bundle was on the order of several micrometers, and this bundle was separated by the ultrasonic method as

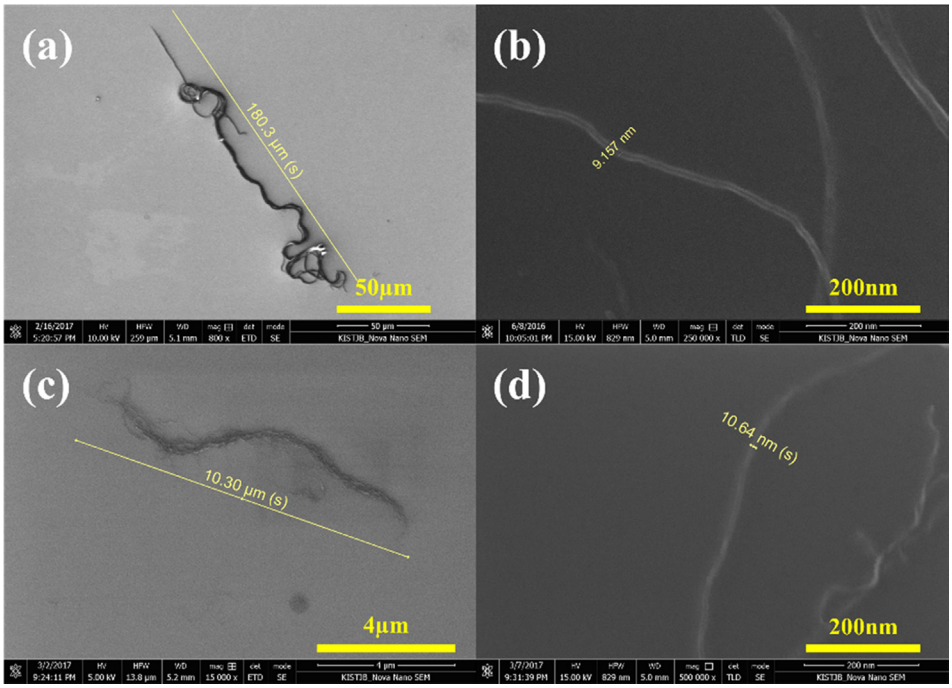

Fig. 1. SEM images of (a), (b) long MWCNTs and (c), (d) short MWCNTs. In (a) and (c), an MWCNT bundle is shown to facilitate measurement of length, whereas in (b) and (d), single MWCNT fibers are shown to facilitate measurement of diameter.

described in Section 2 in order to accurately check the diameter of a single MWCNT fiber. As can be seen in Fig. 1(b) and (d), the diameters of the two types of MWCNTs (i.e., long and short MWCNTs) were almost the same, 9 nm and 10 nm, respectively showing good agreements with the manufacturer's specifications (7–10 nm) [19].

Fig. 2(a) shows the FT-IR spectra of the two types of MWCNTs to enable a comparison of their surface chemistries; from these spectra, both the types of MWCNTs were confirmed to be similar in terms of their overall shape and major peaks, including the O—H peak at 3430 cm^{-1} and the sp^2 C—H peak at 2915 cm^{-1} [20]. The intensity ratio of the OH peak to the sp^2 CH peak was also the same, i.e., 0.93, for both the long and the short MWCNTs. Thus, it can be assumed that the MWCNT dispersion and the corresponding evolution of the composite properties do not originate from the surface chemistry of the MWCNTs. The structural defects of the MWCNTs were measured via Raman analysis, as shown in Fig. 2(b), where both the G peak and the D peak, which are commonly detected in graphite materials, were observed at 1338 and 1572 cm^{-1}, respectively. The D peak represents structural defects and its intensity increases with a strengthening of the sp^3 bond on the MWCNT surface [20,21]. The intensity ratios of the D peak to the G peak (I_D/I_G) were 0.99 and 0.98 for the long and short MWCNTs, respectively, indicating that the defect levels of these two MWCNTs were almost identical.

From the FT-IR and Raman spectra, it was seen that the surface chemistries and defect levels of the two types of MWCNTs were similar; thus, their effects on the composite properties were insignificant. Furthermore, because the diameters of the two types of MWCNTs were nearly identical, the MWCNT length was considered an important morphological parameter governing their dispersion and the composite properties.

3.2. Dispersion of long MWCNTs vis-à-vis short MWCNTs

In order to evaluate the dispersion of MWCNTs in the PA6 polymer, FE-SEM and micro-CT measurements were performed. The FE-SEM images in Fig. 3 show the degree of dispersion of MWCNTs on the fractured surface of the composite; specifically, Fig. 3(a)–(c) and (d)–(f) show the results for long-MWCNT/PA6 (L-PA6) and short-MWCNT/PA6 (S-PA6) composites, respectively. As can be seen in Fig. 3(a) and (d), at a low MWCNT concentration of 1 wt%, even dispersion of MWCNTs was observed in both the L-PA6 and the S-PA6 composites. However, with increasing MWCNT concentration, aggregation was observed: aggregation occurred from 5 wt% onward in the L-PA6 composite and at 10 wt% in the S-PA6 composite. Since the average aspect ratio of the

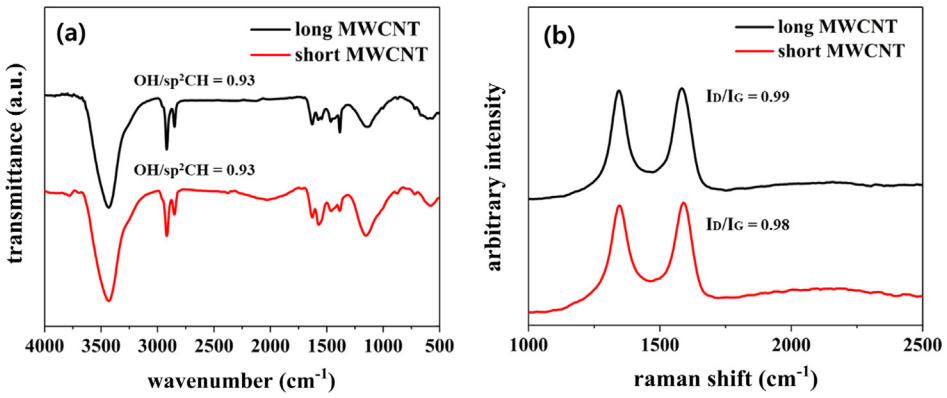

Fig. 2. (a) FT-IR spectra measured from 4000 to 500 cm^{-1} and (b) Raman spectra measured from 1000 to 2500 cm^{-1} for long and short MWCNTs; the peaks at 3430 cm^{-1} and 2915 cm^{-1} in (a) correspond to the O—H peak and sp^2 C—H peak, respectively, whereas those at 1343 cm^{-1} and 1583 cm^{-1} in (b) correspond to the D peak and G peak, respectively.

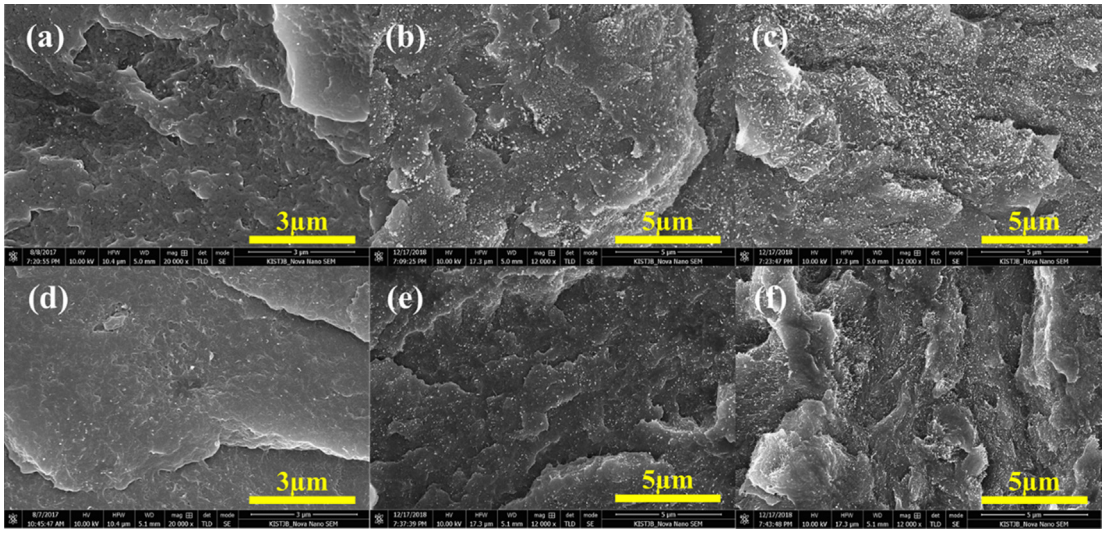

Fig. 3. FE-SEM images of (a)–(c) long-MWCNT/PA6 composite and (d)–(f) short-MWCNT/PA6 composite. The images in (a) and (d), (b) and (e), and (c) and (f) correspond to filler concentrations of 1, 5, and 10 wt%, respectively, dispersed in PA6.

long MWCNTs was 5 times that of the short MWCNTs, the interparticle distance between the strands of the long MWCNTs was short, which resulted in increased aggregation in the long MWCNTs.

Micro-CT is an analytical method capable of nondestructive evaluation of dispersion of fillers in composites. Unlike SEM, which can measure a surface in two dimensions, micro-CT can measure the dispersion of fillers in a relatively wide range of composites in three dimensions. The resolution of the microtomograph used in this study is 700 nm, and if the MWCNTs are evenly dispersed in the PA6 matrix on account of a strong shear force in the internal mixer, the size of the aggregates it will be smaller than the resolution of the microtomograph (700 nm), and the MWCNTs will consequently not be observed. However, when the MWCNTs are aggregated and the aggregate size increases beyond 700 nm, MWCNTs can be observed via micro-CT [22].

Fig. 4(a)–(c) and (d)–(f) show the micro-CT images of the L-PA6 and S-PA6 composites, respectively; the images in Fig. 4(a) and (d), (b) and (e), and (c) and (f) correspond to MWCNT concentrations of 1, 5, and 10 wt%, respectively. In the micro-CT images, the white dots represent MWCNT aggregates; for both the L-PA6 and the S-PA6 composites, the number and size of these aggregates increased as the MWCNT concentration increased. Specifically, micro-CT indicated that aggregation occurred at 5 wt% for the L-PA6 composite and at 10 wt% for the S-PA6 composite, which is in good agreement with the FE-SEM observations in Fig. 3. In other words, from both the micro-CT images and the FE-SEM images, it was found that aggregation occurred at a lower concentration when the long MWCNTs were used whereas dispersion was improved and aggregation occurred to a smaller extent when short MWCNTs were used.

It can thus be concluded that for both the types of MWCNTs, aggregation occurred with increasing MWCNT concentration but that this aggregation began at different concentrations depending on the MWCNT length. Therefore, the length of MWCNTs is an important morphological factor governing their dispersion, and it is consequently thought to be a crucial factor influencing the physical properties of the composite material.

3.3. Mechanical, thermal, and electrical properties

3.3.1. Mechanical properties

Fig. 5 shows the evolutions of the tensile strength and Young's modulus with the MWCNT concentration and length. With an increase in the MWCNT concentration from a low value, the tensile strength and

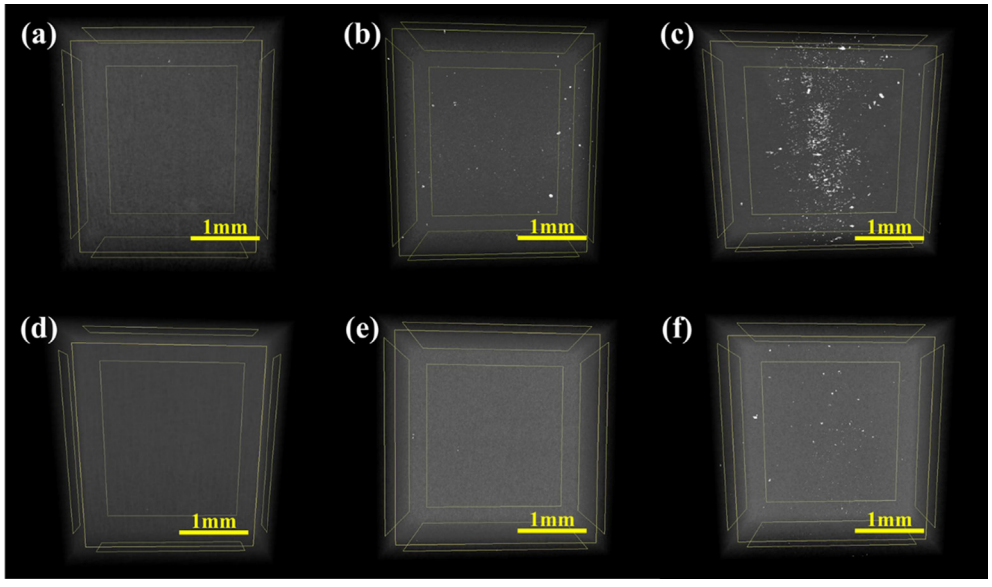

Fig. 4. Micro-CT images of (a)–(c) long-MWCNT/PA6 composite and (d)–(f) short-MWCNT/PA6 composite. The images in (a) and (d), (b) and (e), and (c) and (f) correspond to filler concentrations of 1, 5, and 10 wt%, respectively, dispersed in PA6. The resolution of the microtomograph is 700 nm, and the MWCNT filler is observed as white dots when the aggregates become larger than 700 nm in size.

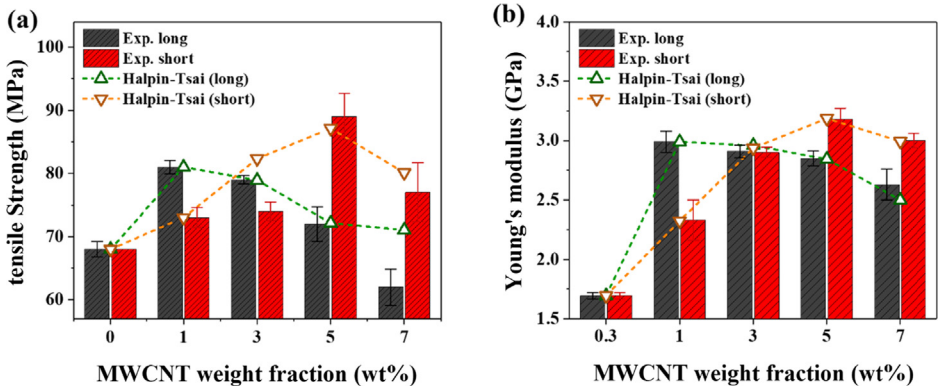

Fig. 5. Tensile strength (a) and Young's modulus (b) plotted against MWCNT concentration for long- and short-MWCNT/PA6 composites under uniaxial tension at room temperature at constant engineering strain rate of 5 mm/min.

Young's modulus increased, attained maximum values, and subsequently decreased. It is notable that the concentration at which both the tensile strength and the Young's modulus attained maximum values depended strongly on the MWCNT length. For example, the L-PA6 composite showed the maximum tensile strength at 1 wt%, whereas the S-PA6 composite showed the maximum tensile strength and Young's modulus at 5 wt%. In this respect, the MWCNT length is an important morphological factor for the tensile properties of the composite.

As shown in Fig. 5, at the concentration of 1 wt%, the L-PA6 composite showed 12% higher tensile strength and 40% higher Young's modulus than the S-PA6 composite (81 MPa, 3.0 GPa and 73 MPa, 2.3 GPa for L-PA6 and S-PA6, respectively). The tensile strain–stress curves at 1 wt% in Fig. S2 reveal more distinct differences, where the L-PA6 composite shows elastic deformation until brittle failure whereas the S-PA6 composite shows plastic deformation after yielding. At this low concentration, the MWNCTs were uniformly dispersed without any aggregation regardless of the length (see the FE-SEM and micro-CT images in Figs. 3 and 4, respectively); therefore, the difference in tensile properties seems to be dominated by the aspect ratio [12,23–26]. That is, under uniform dispersion, the composite with long MWCNTs shows better tensile performance because of its high force transfer efficiency [27].

However, contrary to the expectation that long MWCNTs would outperform short MWCNTs in terms of the force transfer efficiency, the short MWCNTs showed superior performance as a filler as their concentration increased. For example, the tensile properties of the L-PA6 composite decreased from 3 wt% onward whereas those of the S-PA6 composite continued to increase up until 5 wt%, and the latter ended up with the highest tensile strength and Young's modulus in this study. The superior performance of the short MWCNTs at higher concentrations originated from their even dispersion in the composite. The concentrations at which the tensile performance began degrading were 3 wt% and 7 wt% for the L-PA6 composite and S-PA6 composite, respectively, as shown in Fig. 5; these results are in good agreement with the FE-SEM and micro-CT observations. That is, in the case of the L-PA6 composite, poor dispersion and corresponding aggregation from 3 wt% onward caused a decrease in the area of the MWCNT–matrix interface, which, in turn, led to a sharp decrease in the tensile properties. However, the S-PA6 composite showed uniform dispersion up until 5 wt%, which resulted in its highest tensile strength and Young's modulus. In conclusion, when the MWCNTs are uniformly dispersed, the tensile properties are predominantly influenced by their aspect ratio. On the other hand, because of the occurrence of aggregation with an increase in the MWCNT concentration, dispersion becomes a major influencing factor.

For more comprehensive and in-depth analysis, the theoretical values were calculated using the modified Halpin-Tsai equation [28,29] as in Eq. (2) and compared with the experimental measurements.

$$E_c = \left[\frac{1+\psi\eta V_f}{1-\eta V_f}\right]E_m, \quad \eta = \frac{(\alpha E_f/E_m)-1}{(\alpha E_f/E_m)+\psi}, \quad \psi = 2\frac{l}{d}e^{-aVf-b} \tag{2}$$

where E_c, E_m and E_f indicates the Young's modulus of composite, matrix and MWCNT, while V_f and α are the volume fraction and orientation factor of MWCNT. Ψ represents the exponential shape factor, where the parameters of a and b are closely related to the degree of filler aggregation. That is, the higher the values of the parameters, the greater the aggregation, which consequently leads to nonlinear behaviors of mechanical performance with increasing MWCNT contents. The equation for tensile strength exhibits itself as the exactly same form, and the detailed calculations are explained in the Supporting Information. As a result, the predictions were well overlapped with the experimental observations, where higher values of a and b were obtained for long MWCNT; a: 75, b: 4.9 (long) and a: 70, b: 2.7 (short) for Young's modulus, and a: 200, b: 4.5 (long) and a:170, b:0.3 (short) for tensile strength. Of particular interest is the lower a and b values for short MWCNT. That is, the modified Halpin-Tsai equation predictions revealed that short MWCNTs were more uniformly dispersed than long MWCNTs, which is in good agreement with the experimental observations through SEM and micro-CT.

3.3.2. Thermal conductivity

Fig. 6 shows the results of thermal conductivity measurements at various MWCNT concentrations and lengths. As the MWCNT concentration increased, the thermal conductivity of both the L-PA6 and the S-PA6 composites improved. However, the degree of improvement was higher for the L-PA6 composite at all the concentrations. Since the surface chemistry and defect levels of the two types of MWCNTs were

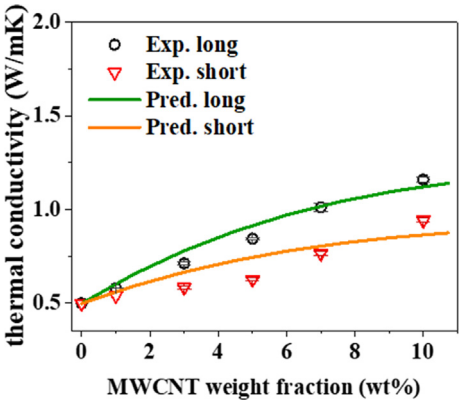

Fig. 6. Thermal conductivity plotted against MWCNT concentration for long- and short-MWCNT/PA6 composites. For each concentration, measurements were performed 5 times at 30 min intervals.

similar to each other as confirmed by the FT-IR and Raman spectra, these MWCNTs differed only in terms of the length and degree of dispersion. In contrast to a previously reported result that uniform dispersion of MWCNTs was the main factor influencing thermal conductivity [25], our observations indicated that dispersion had no significant effect on thermal conductivity. For instance, the thermal conductivity did not decrease but rather increased even at concentrations at which non-uniform dispersion and aggregation occurred; this behavior was specifically observed at concentrations of 5 wt% and 10 wt% for the L-PA6 and S-PA6 composites, respectively. In conclusion, the thermal conductivity was dominantly influenced by the length rather than the degree of dispersion, which is attributed to the reduction in phonon scattering due to a reduction in the contact interface area for long MWCNTs [19,30,31].

The present experimental results for MWCNT/PA6 composites were compared with a micromechanics-based model using the following Eq. (3), as shown in Fig. 6.

$$\bar{\mathbf{K}}^{*} = \mathbf{K}_0 \cdot \left[\mathbf{I} + \sum_{r=0}^{4} \{\phi_r (\mathbf{S}_r + \mathbf{A}_r)^{-1} \cdot [\mathbf{I} - \phi_r \mathbf{S}_r \cdot (\mathbf{S}_r + \mathbf{A}_r)^{-1}]^{-1}\} \right] \tag{3}$$

where $\bar{\mathbf{K}}^{*}$ is the effective thermal conductivity of composite containing 3D randomly oriented and variously aggregated MWCNTs. Detailed descriptions of the additional constants are included in the previous literature [19]. The values measured in this experiments were applied for the material parameters of the analysis. In this simulation, it was assumed that the interfacial characteristic of the MWCNT was the same regardless of the length; however, the filler aggregation was affected by its length. Consequently, it was revealed that longer MWCNT led to a higher thermal conductivity when the same concentration was incorporated, which is well agreed with the experimental observations. The improvement ratio of the thermal conductivity according to the filler concentration gradually decreased, finally converging to a specific value.

3.3.3. Electrical conductivity

Fig. 7 shows the results of electrical conductivity measurements at different MWCNT concentrations and lengths. Irrespective of the MWCNT length, the percolation threshold was reached at a concentration of around 1 wt%. In order for electrical percolation to occur, the distance between MWCNTs in a composite must be small enough for the formation of an electrical path. Thus, uniform dispersion of MWCNTs is considered a major physical factor that governs the electrical percolation of a nanocomposite [5,11,32]. The fact that both the L-PA6 and the S-PA6 composites reached the percolation threshold indicates that the MWCNTs were uniformly dispersed in the composites at the concentration of 1 wt%. After the percolation threshold was reached, the electrical conductivities of both the composites showed similar tendencies. As a result, the composite materials had a sufficient electrical path for electron transfer at an MWCNT concentration of 1 wt %, with the effects of the MWCNT length and dispersion being negligible.

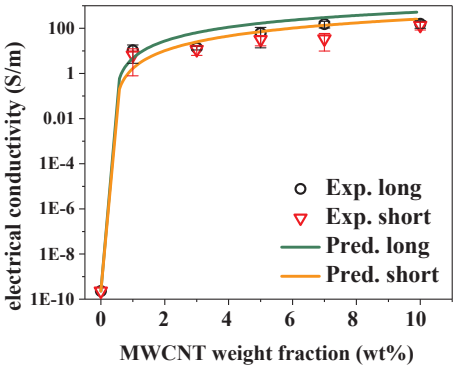

Fig. 7. Electrical conductivity plotted against MWCNT concentration for long- and short-MWCNT/PA6 composites. Measurements were performed at least 30 times for each concentration and the mean value was calculated.

The electrical conductivity was also analyzed through a theoretical formula, as shown in Fig. 7. The electrical conductivity of 3D randomly oriented and aggregated the MWCNT/PA6 composite can be derived through the effective medium model as [22]

$$\phi_0 [(\mathbf{L}_0 - \mathbf{L}_e)^{-1} + \mathbf{S}_0 \mathbf{L}_e^{-1}]^{-1} + \phi_1 [(\mathbf{L}_1 - \mathbf{L}_e)^{-1} + \mathbf{S}_1 \mathbf{L}_e^{-1}]^{-1} = 0 \tag{4}$$

where $\mathbf{L}_e$ denotes the effective conductivity tensor, which can be obtained by solving Eq. (4). The definition of constants in Eq. (4) and the modeling process are described in more detail in the previous literature [22]. The experimentally measured parameters were applied to the model. The simulation calculations indicated that the incorporation of longer MWCNT resulted in a higher electrical conductivity at percolation threshold and later, which is well overlapped with the experimental observations. However, it was not so much affected by the filler length in the matrix, contrary to the case of the thermal conductivity.

4. Conclusion

In order to investigate the effects of MWCNT morphology on the properties of an MWCNT-incorporated polymer composite, two kinds of MWCNTs with similar surface chemistry and thickness but with different lengths were mixed with a PA6 polymer matrix for composite fabrication via a melt-compounding method. FE-SEM and micro-CT observations revealed that the length of MWCNTs strongly influenced their dispersion state in the composite, where a short-MWCNT/PA6 composite showed more uniform dispersion up to higher MWCNT concentrations. The mechanical performance, electrical conductivity, and thermal conductivity of the fabricated composite were measured in order to understand the correlations among the MWCNT length, dispersion state, and composite properties. The following conclusions were drawn. (1) The aspect ratio has a dominant effect on the tensile properties of the composite when the MWCNTs are uniformly dispersed; thus, better tensile performance is achieved for the composite with long MWCNTs. However, as the MWCNT concentration increases, dispersion becomes a major physical factor influencing the tensile performance and the use of short MWCNTs is more effective because their dispersion is more uniform. (2) Thermal conductivity increases with increasing MWCNT concentration and shows a larger improvement for the composite with long MWCNTs, since these MWCNTs form a smaller interface with the polymer and accordingly reduce phonon scattering. The effects of dispersion and aggregation on thermal conductivity are negligible. (3) Above 1 wt%, at which concentration the percolation threshold is reached, the MWCNT length does not have a significant effect on the electrical conductivity of the composite. In this study, the mechanical, electrical, and thermal properties of an MWCNT-incorporated polymer composite were systematically examined in order to correlate them with the length and dispersion of the MWCNTs. We believe that the fundamental understanding gained from this study can be applied as design guidelines for morphology selection of MWCNTs for a wide range of applications.

Declaration of Competing Interest

The authors declare no competing interest.

Acknowledgements

This study was supported by the Korea Institute of Science and Technology (KIST) Institutional Program (2Z05720). In addition, this material is based upon work supported by the Ministry of Trade, Industry & Energy of Korea under Industrial Technology Innovation

Program (10082586), and by the Ministry of Education, National Research Foundation of Korea (NRF) under Basic Science Research Program (2017R1C1B5077037).

Appendix A. Supplementary material

Supplementary data to this article can be found online at https://doi.org/10.1016/j.compositesa.2019.105542.

References

[1] Ajayan PM, Tour JM. Materials science: nanotube composites. Nature 2007;447(7148):1066.
[2] Moniruzzaman M, Winey KI. Polymer nanocomposites containing carbon nanotubes. Macromolecules 2006;39(16):5194–205.
[3] Al-Saleh MH, Sundararaj U. Review of the mechanical properties of carbon nanofiber/polymer composites. Compos Part A Appl Sci Manuf 2011;42(12):2126–42.
[4] Han Z, Fina A. Thermal conductivity of carbon nanotubes and their polymer nanocomposites: a review. Prog Polym Sci 2011;36(7):914–44.
[5] Spitalsky Z, Tasis D, Papagelis K, Galiotis C. Carbon nanotube–polymer composites: chemistry, processing, mechanical and electrical properties. Prog Polym Sci 2010;35(3):357–401.
[6] Cadek M, Coleman J, Barron V, Hedicke K, Blau W. Morphological and mechanical properties of carbon-nanotube-reinforced semicrystalline and amorphous polymer composites. Appl Phys Lett 2002;81(27):5123–5.
[7] Liu T, Phang IY, Shen L, Chow SY, Zhang W-D. Morphology and mechanical properties of multiwalled carbon nanotubes reinforced nylon-6 composites. Macromolecules 2004;37(19):7214–22.
[8] Hu M, Yu D, Wei J. Thermal conductivity determination of small polymer samples by differential scanning calorimetry. Polym Test 2007;26(3):333–7.
[9] T'Joen C, Park Y, Wang Q, Sommers A, Han X, Jacobi A. A review on polymer heat exchangers for HVAC&R applications. Int J Refrig 2009;32(5):763–79.
[10] Dean JA. Lange's handbook of chemistry. New York; London: McGraw-Hill, Inc.; 1999.
[11] Bauhofer W, Kovacs JZ. A review and analysis of electrical percolation in carbon nanotube polymer composites. Compos Sci Technol 2009;69(10):1486–98.
[12] Ma P-C, Siddiqui NA, Marom G, Kim J-K. Dispersion and functionalization of carbon nanotubes for polymer-based nanocomposites: a review. Compos Part A Appl Sci Manuf 2010;41(10):1345–67.
[13] Yu J, Choi HK, Kim HS, Kim SY. Synergistic effect of hybrid graphene nanoplatelet and multi-walled carbon nanotube fillers on the thermal conductivity of polymer composites and theoretical modeling of the synergistic effect. Compos Part A Appl Sci Manuf 2016;88:79–85.
[14] Funck A, Kaminsky W. Polypropylene carbon nanotube composites by in situ polymerization. Compos Sci Technol 2007;67(5):906–15.
[15] Wang Z, Liang Z, Wang B, Zhang C, Kramer L. Processing and property investigation of single-walled carbon nanotube (SWNT) buckypaper/epoxy resin matrix nanocomposites. Compos Part A Appl Sci Manuf 2004;35(10):1225–32.
[16] Xu Y, Ray G, Abdel-Magid B. Thermal behavior of single-walled carbon nanotube polymer–matrix composites. Compos Part A Appl Sci Manuf 2006;37(1):114–21.
[17] Qian H, Bismarck A, Greenhalgh ES, Shaffer MS. Carbon nanotube grafted carbon fibres: a study of wetting and fibre fragmentation. Compos Part A Appl Sci Manuf 2010;41(9):1107–14.
[18] De Volder MF, Tawfick SH, Baughman RH, Hart AJ. Carbon nanotubes: present and future commercial applications. Science 2013;339(6119):535–9.
[19] Kim SY, Jang HG, Yang C-M, Yang B. Multiscale prediction of thermal conductivity for nanocomposites containing crumpled carbon nanofillers with interfacial characteristics. Compos Sci Technol 2018;155:169–76.
[20] Kim UJ, Furtado CA, Liu X, Chen G, Eklund PC. Raman and IR spectroscopy of chemically processed single-walled carbon nanotubes. J Am Chem Soc 2005;127(44):15437–45.
[21] Bokobza L, Zhang J. Raman spectroscopic characterization of multiwall carbon nanotubes and of composites. Express Polym Lett 2012;6(7).
[22] Yang B, Jang J-u, Eem S-H, Kim SY. A probabilistic micromechanical modeling for electrical properties of nanocomposites with multi-walled carbon nanotube morphology. Compos Part A Appl Sci Manuf 2017;92:108–17.
[23] Coleman JN, Khan U, Gun'ko YK. Mechanical reinforcement of polymers using carbon nanotubes. Adv Mater 2006;18(6):689–706.
[24] Coleman JN, Khan U, Blau WJ, Gun'ko YK. Small but strong: a review of the mechanical properties of carbon nanotube–polymer composites. Carbon 2006;44(9):1624–52.
[25] Song YS, Youn JR. Influence of dispersion states of carbon nanotubes on physical properties of epoxy nanocomposites. Carbon 2005;43(7):1378–85.
[26] Misiego CR, Pipes RB. Dispersion and its relation to carbon nanotube concentration in polyimide nanocomposites. Compos Sci Technol 2013;85:43–9.
[27] Qian D, Dickey EC, Andrews R, Rantell T. Load transfer and deformation mechanisms in carbon nanotube-polystyrene composites. Appl Phys Lett 2000;76(20):2868–70.
[28] Montazeri A, Javadpour J, Khavandi A, Tcharkhtchi A, Mohajeri A. Mechanical properties of multi-walled carbon nanotube/epoxy composites. Mater Des 2010;31(9):4202–8.
[29] Yeh M-K, Tai N-H, Liu J-H. Mechanical behavior of phenolic-based composites reinforced with multi-walled carbon nanotubes. Carbon 2006;44(1):1–9.
[30] Park JG, Cheng Q, Lu J, Bao J, Li S, Tian Y, et al. Thermal conductivity of MWCNT/epoxy composites: the effects of length, alignment and functionalization. Carbon 2012;50(6):2083–90.
[31] Kim HS, Jang J-u, Yu J, Kim SY. Thermal conductivity of polymer composites based on the length of multi-walled carbon nanotubes. Compos Part B Eng 2015;79:505–12.
[32] Li J, Ma PC, Chow WS, To CK, Tang BZ, Kim JK. Correlations between percolation threshold, dispersion state, and aspect ratio of carbon nanotubes. Adv Funct Mater 2007;17(16):3207–15.